Stabilization of Hydroxide Ions at the Interface of a Hydrophobic Monolayer on Water via Reduced Proton Transfer

Shanshan Yang,[1] Mohan Chen,[2] Yudan Su,[1] Jianhang Xu,[3] Xifan Wu,[3,4,*] and Chuanshan Tian[1,†]
[1]State Key Laboratory of Surface Physics and Key Laboratory of Micro- and Nano-Photonic Structures (MOE), Department of Physics, Fudan University, Shanghai 200433, China
[2]CAPT, HEDPS, College of Engineering, Peking University, Beijing 100871, China
[3]Department of Physics, Temple University, Philadelphia, Pennsylvania 19122, USA
[4]Institute for Computational Molecular Science, Temple University, Philadelphia, Pennsylvania 19122, USA

(Received 17 June 2020; accepted 25 August 2020; published 9 October 2020)

We report a joint study using surface-specific sum-frequency vibrational spectroscopy and *ab initio* molecular dynamics simulations, respectively, on a pristine hydrophobic (sub)monolayer hexane-water interface, namely, the hexane/water interface with varied vapor pressures of hexane and different *p*Hs in water. We show clear evidence that hexane on water revises the interfacial water structure in a way that stabilizes the hypercoordinated solvation structure and slows down the migration of hydroxide ion (OH^-) relative to that in bulk water. This mechanism effectively attracts the OH^- to the water-hydrophobic interface with respect to its counterion. The result illustrates the striking difference of proton transfer of hydrated OH^- at the interface and in the bulk, which is responsible for the intrinsic charging effect at the hydrophobic interface.

DOI: 10.1103/PhysRevLett.125.156803

Introduction.—Hydroxide ions are one of the most fundamental ionic species in water and are of great importance in diverse phenomena in physics, chemistry, and biology. Their excess at an interface strongly depends on the local hydrogen (H) -bonding network as well as the nature of the dynamic proton transfer [1], which can change the local *p*H and affect the surface chemistry, such as reaction rate and pathway [2–5]. There has been a lingering puzzle about the propensity of hydrated OH^- at the hydrophobic material-water interface. Early macroscopic measurements inferred an excess of OH^- residing at the hydrophobic interface [6–9]. This was later supported by surface-specific optical spectroscopic measurements [10,11]. However, some other experimental and theoretical studies attributed the appearing interfacial charge to contamination [12–15], anisotropic dipole potential [16,17], or charge redistribution [18] at the interface. The problem lies in the fact that most of the early measurements were conducted at the hydrophobic interface formed via water in contact with a bulk of hydrophobic material [6,7,9,14,19] or a substrate coated with hydrophobic thin film [10,12,13,15]. However, it was questioned that the surface charge might stem from contamination of ionic surfactant molecules at the interface [14,20] or from surface chemistry of the supporting substrate [13,15,21]. Obviously, a pristine hydrophobic interface and surface-sensitive technique is required to revisit the mechanism of the surface charging effect.

The theoretical investigation of the surface propensity of OH^- at a hydrophobic interface is nontrivial because it strongly depends on proton transfer (PT) events in the H-bonding network at the interface and modeling PT in the H-bonding network has long been a lingering challenge [22,23]. Difficulties are rooted in the highly complex structure of the H-bonding network dynamically revised in the interfacial water which sensitively affects the PT. Major progress in modeling PT was made using *ab initio* molecular dynamics (AIMD) simulations [24]. It revealed that OH^- forms two types of solvation complexes in bulk water: the tetrahedral (or three-coordinated) $OH^-(H_2O)_3$ and the hypercoordinated $OH^-(H_2O)_4$ [24]. Diffusion of OH^- happens via rapid PTs through H bonds in the $OH^-(H_2O)_3$ complex (the *active* mode) but halts when it adopts the $OH^-(H_2O)_4$ solvation structure (the *asleep* mode) [1,24]. Conversion between the two modes is thermally excited. It is of fundamental importance to learn the nature of PT of OH^- at the interface versus in bulk and whether it leads to OH^- excess at the hydrophobic interface. A pioneering AIMD work has pointed out that the amphiphilic nature of OH^- may result in negatively charged hydrophobic water surfaces [25], but the mechanism for stabilization of OH^- in connection with its solvation structure and PT process near the surface has not been addressed [26].

In this Letter, we report a combined theoretical and experimental study of a hydrophobic gas-water interface theoretically by AIMD simulation and experimentally by sum-frequency vibrational spectroscopy (SFVS). Hexane was chosen as the hydrophobic molecular gas because it adsorbed on a water surface via Van der Waals

interaction forming a (sub)monolayer without introducing bonding to water or OH^-. We found unanimously that the surface density of OH^- at the interface was greatly enhanced after adsorption of hexane molecules on water revising the surface structure. Our AIMD simulation revealed that the enhanced OH^- surface density originates from the hexane-incorporated H-bonding network at the interface, where OH^- tends to form a stable hypercoordinated structure that greatly suppresses the mobility and PT rate of OH^- in comparison with OH^- in bulk water.

Results and discussion.—Figure 1(a) describes our experimental arrangement, with details provided in literature [27,28] the Supplemental Material [29]. Water with a specific *p*H held by a cell in the chamber was under variable pressure of hexane gas, which was directed into the chamber by the gas line after being filtered by the NaOH (aq.) solution. The hexane vapor pressure was monitored by the Fourier-transform IR spectrometer. NaOH was used to prepare all the basic solutions in this work. Sum-frequency vibrational spectroscopy from the hexane-water interface was carried out in the reflected direction [30,31].

The sum-frequency (SF) vibrational spectra [describing $|\chi^{(2)}_{S,\mathrm{eff}}(\omega)|^2$, with $\chi^{(2)}_{S,\mathrm{eff}}(\omega)$ being the surface nonlinear susceptibility] taken with neat water (*p*H 5.6) and water of *p*H 10.0 under different hexane pressures are displayed in Fig. 1(b). Characteristic peaks of the methyl group symmetric and antisymmetric stretching modes at 2880 and 2960 cm^{-1} for adsorbed hexane and the broad band with a narrow peak in the range of 3000–3800 cm^{-1} for OH stretches of interfacial water can be seen in the figure. As hexane vapor pressure increases, both CH_3 stretching modes appear stronger, indicating increasing hexane coverage on the water surface. The Van der Waals interaction between hexane and water is weak; therefore the orientation order of sub-monolayer coverage of hexane on water is poor, as suggested by Monte Carlo simulation. Meanwhile, the neat water spectrum [top in Fig. 1(b)] clearly changes with the hexane vapor pressure. It must come from the modification

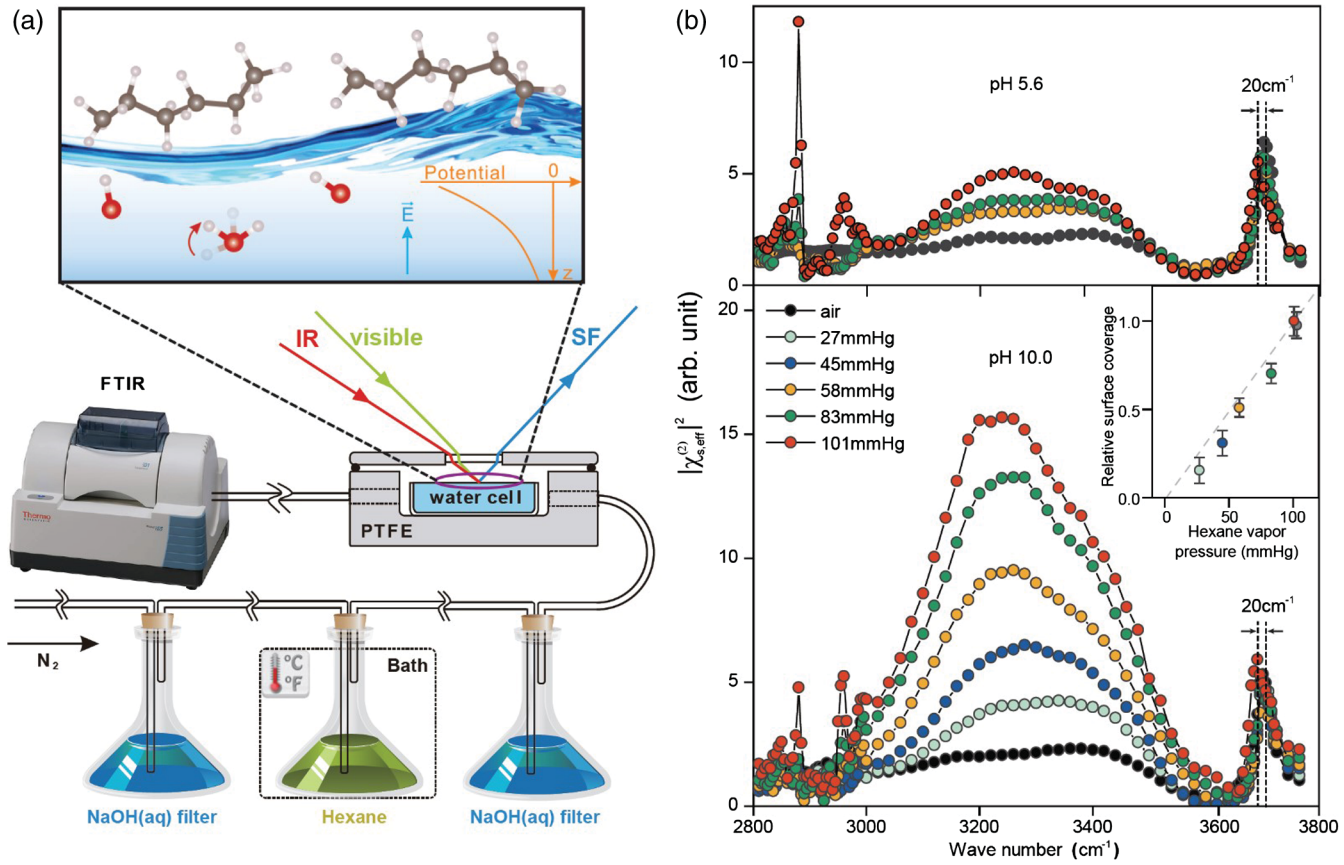

FIG. 1. Experimental arrangement and intensity spectra of SFVS for the hexane gas-water interface. (a) Sketch of the experimental setup: Hexane mixed with nitrogen (99.999%) was led into the chamber by a gas line after filtering by NaOH(aq.) solution, and its vapor pressure in the chamber was monitored by the Fourier-transform IR spectrometer. Enlarged view shows schematic structure of the adsorbed hexane molecules and surface electric potential set by adsorption of ions. (b) Upper and lower panels display SFVS intensity spectra of the hexane-water interfaces of water solution at *p*H 5.6 and *p*H 10.0, respectively, under different hexane vapor pressures. The largest redshift of dangling OH is ~20 cm^{-1} with reference to the case without hexane, as indicated by the dashed lines. Inset of (b) shows hexane coverage versus hexane vapor pressure at *p*H 10.0.

of the interfacial water structure by the adsorbed hexane molecules and has been interpreted as due to an increased water surface area caused by hexane adsorption [32] (see Fig. S5 in the Supplemental Material [29] for more details).

For both pH 5.6 and pH 10.0 water, the dangling OH mode of water that serves as a spectral signal of a hydrophobic water interface is clearly visible [22] initially at 3700 cm^{-1} in the absence of hexane, then redshifted as the hexane vapor pressure increases, and finally reaching 3680 cm^{-1} upon saturated adsorption of hexane. The redshift is the result of an interaction between hexane and surface water molecules in close contact [10,23]. Actually, the dangling OH peak in all spectra could be decomposed into two peaks, one at 3680 cm^{-1} and the other at 3700 cm^{-1}. The former comes from dangling OHs that are in contact with hexane and the latter from OHs protruding into air. Thus, the strength of the 3680 cm^{-1} can be used to estimate the hexane coverage (see Sec. S2 of the Supplemental Material [29]). With the given pH, the hexane coverage increases almost linearly with the hexane vapor pressure until saturation [inset of Fig. 1(b); the coverage approaches one monolayer at 101 mm Hg], while the orientation of the adsorbed hexane molecules appears to depend on the pH, as evidenced by the changes of the CH_2 and CH_3 spectral features with the pH in Fig. S4 of the Supplemental Material [29] (see also Secs. S4 and Sec. S7 of the Supplemental Material) [33–36].

In the bonded-OH stretching range (3000–3600 cm^{-1}), the SF spectrum increases with the hexane vapor pressure; it shows a much stronger growth for water at pH 10.0 than at pH 5.6 [Fig. 1(b)]. As hexane reaches ~1.0 monolayer (101 mm Hg), the latter is 2 times stronger than that of the air-water interface, but the former appears nearly 1 order of magnitude larger. The interface of hexane on neat water (pH 5.6) is found to be practically charge neutral because its SF spectrum is not affected by ion solvation in water (see Fig. S5 in the Supplemental Material [29]). At pH 10.0, the spectral enhancement in the bottom of Fig. 1(b) is reduced after adding salt in the water, indicating the existence of an electric double layer (EDL) at the hexane-water interface [37,38]. The surface charges set up an EDL in which the dc electric-field-induced polarization of water contributes to the observed SF spectral change. To be sure that the spectral change was not from contamination of the hexane gas, we passed the gas through NaOH(aq.) solutions to remove small amphiphilic molecules such as acetic acid and found no effect on the spectrum. We also evacuated the hexane gas from the sample chamber and found no trace of residual amphiphilic molecules left on the water surface (see Sec. S3 of the Supplemental Material [29]).

Negative OH^- is expected to be attracted by hexane to the surface of water at pH 10.0 as in the case of alkane chains facing water [10]. This can be confirmed by the $\mathrm{Im}\chi^{(2)}_{S,\mathrm{eff}}(\omega)$ spectra deduced from $\chi^{(2)}_{S,\mathrm{eff}}(\omega)$ with the help of a few phase measurements at selected IR frequencies on

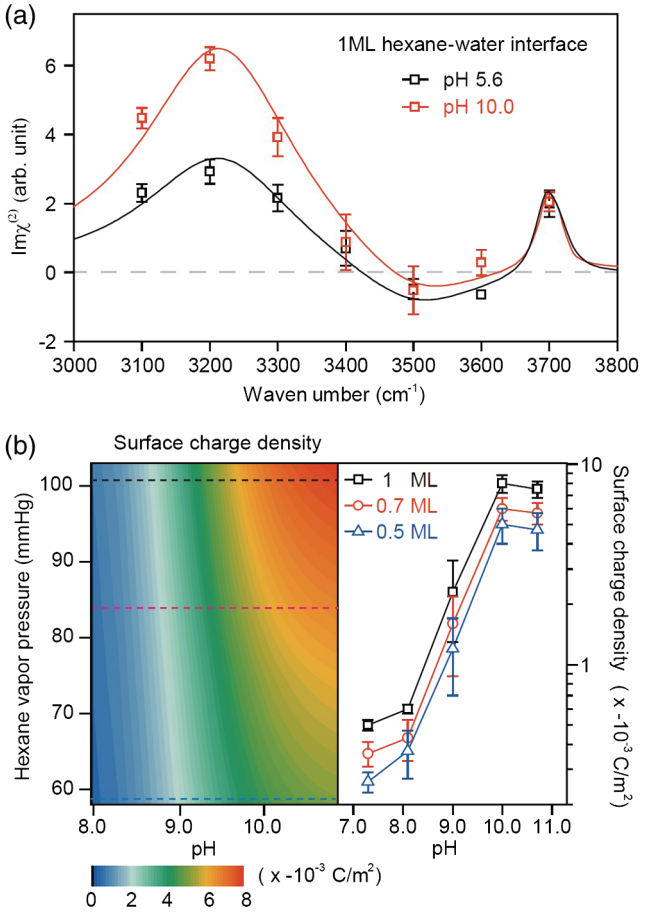

FIG. 2. Results of spectral analysis. (a) $\mathrm{Im}\chi^{(2)}_{S,\mathrm{eff}}(\omega)$ spectra in the OH stretching region of the hexane-water interface for water at pH 5.6 and pH 10.0 under 101 mm Hg hexane vapor pressure deduced from observed $|\chi^{(2)}_{S,\mathrm{eff}}(\omega)|^2$ with the help of phase measurements at discrete IR frequencies. (b) 3D plot describing surface charge (OH^-) density versus hexane vapor pressure and OH^- concentration in bulk water; surface charge density versus pH at three different hexane vapor pressures are presented in the right panel and also indicated by three dashed lines in the 3D plot, where 0.5, 0.7, and 1 monolayer surface coverage of hexane on water corresponds to 58, 83, and 101 mm Hg vapor pressure.

$\chi^{(2)}_{S,\mathrm{eff}}(\omega)$ [39,40]. As seen in Fig. 2(a), the $\mathrm{Im}\chi^{(2)}(\omega)$ spectrum becomes more positive with 0.1 mM NaOH in neat water to yield pH 10.0, indicating the presence of negative surface charges that create an EDL of water molecules with field-induced net O → H orientation toward the surface [37,41,42].

Quantitatively, we can extract the surface density of OH^- at the hexane-water interface from the measured $\chi^{(2)}_{S,\mathrm{eff}}(\omega)$ spectrum using a recently developed method [37,43]. For surface OH^- density less than ~0.05 e/nm^2, the change of $\chi^{(2)}_{S,\mathrm{eff}}(\omega)$ due to surface OH^- is given by

$$\Delta\chi^{(2)}_{S,\mathrm{eff}}(\omega) = \chi^{(3)}_B \int_{0^+}^{\infty} E_{\mathrm{dc}}(z) e^{i\Delta k_z z} dz, \qquad (1)$$

where $\chi_B^{(3)}$ describing the third-order nonlinear susceptibility of bulk water is known from previous measurements, $E_{\mathrm{dc}}(z)$, which denotes the dc electric field along the surface normal $\hat{z}$ and set up in the EDL by the surface charges, is related to the surface charge density by the Guoy-Chapman theory; Δk_z representing a phase mismatch of the SFVS process along z can be obtained from the experimental beam geometry. Equation (1) allows the deduction of the surface charge density from the measured $\Delta\chi^{(2)}_{S,\mathrm{eff}}(\omega)$ spectrum with known $\chi_B^{(3)}$ (see Sec. S5 of the Supplemental Material [29]).

Using the abovementioned procedures, we obtain the surface density of OH^- versus the pH and hexane vapor pressure as presented in 3D contour plots in Fig. 2(b). The OH^- surface density grows rapidly with both the hexane pressure and bulk pH. The data of OH^- surface density versus pH from three dashed line cuts for three different hexane coverages of 0.5, 0.7, 1.0 monolayer on water in the 3D contour plot are shown explicitly on the right of Fig. 2(b). At the same pH, higher hexane surface coverage results in larger surface OH^- density. At 1.0 monolayer coverage of hexane and pH of 10.0, the surface density of OH^- reaches $\sim 8\ \mathrm{mC/m^2}$, which is consistent with the value reported by Beattie and Djerdjev on purified oil emulsion in water [9]. We note that the three lines on the right of Fig. 2(b) can actually converge into one if they are normalized to their respective saturation value at high pHs (see Fig. S7 in the Supplemental Material [29]). This indicates that under different hexane coverage, the adsorption kinetics is the same; a change of hexane coverage simply changes the number of adsorption sites for OH^-. Assuming each hexane molecule occupies 31 $\mathrm{Å}^2$ on the water surface [44], we estimated that each adsorbed OH^- should be associated with roughly five adsorbed hexane molecules at the hexane-water interface.

To understand how adsorbed hexane can induce OH^- to the hexane-water interface, we investigate the dynamics of OH^- at the monolayer hexane-water interface by AIMD (see Sec. S1 of the Supplemental Material [29] for setups) [45–48]. As shown in Fig. 3, frequent PTs (spikes in the figure) between 0 and 18 ps indicate high mobility of OH^- in bulk. Solvated in the bulk liquid water, OH^- adopts the so-called hypercoordination as the most stable configuration in which the lone pair electrons of OH^- can accept four water molecules, forming a planarlike structure [21] also known as the *asleep* mode of OH^- because it forbids PT from occurring [1,49,50]. However, influenced

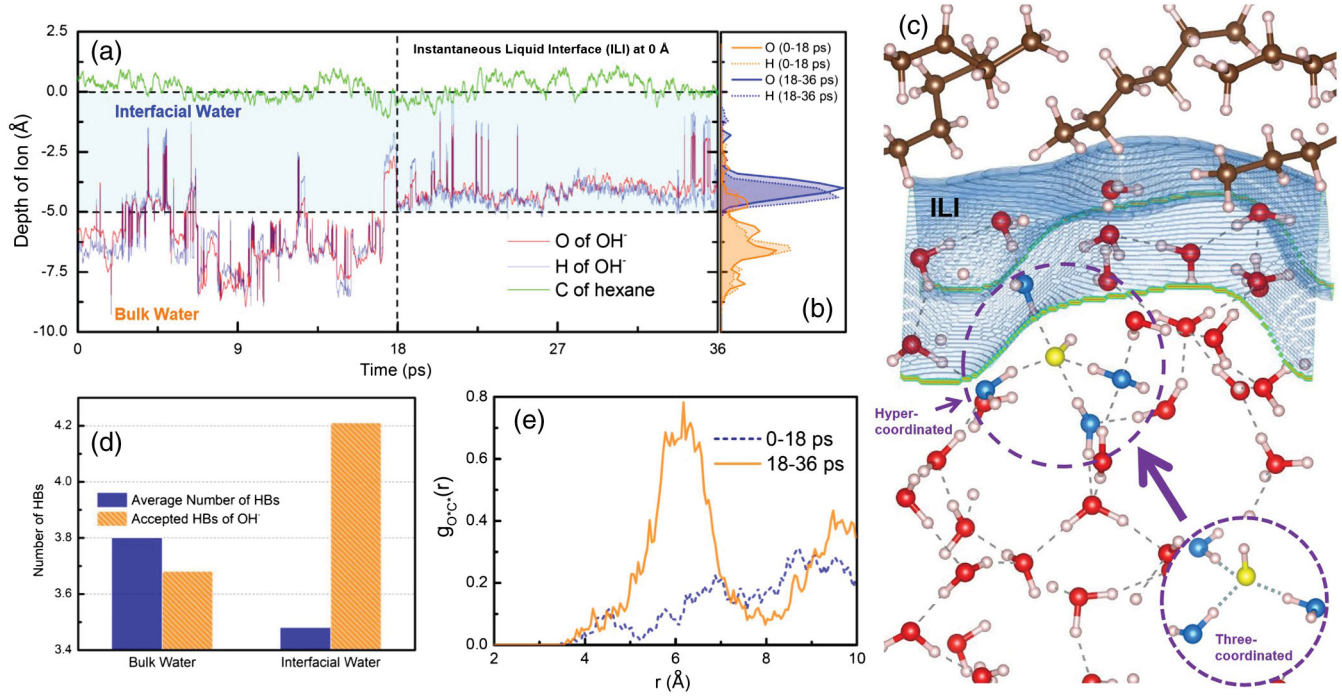

FIG. 3. AIMD simulations of the water-hexane interface. (a) Depth positions of O and H of OH^- and C in hexane with respect to the instantaneous liquid interface (ILI, set as zero) as a function of the time. Boundary between bulk and interfacial (blue region) water is taken at depth of −5.0 Å. (b) Distributions of O and H of OH^- in depth in the interface and bulk regions. (c) Snapshot illustration of H-bonding network of water with OH^- in the water-hexane interfacial region. C in brown, H in white, OH^- with O in yellow, and water molecules generally with O in red, but those coordinated with OH^- in blue. Blue mesh refers to the ILI. (d) Number of H bonds (HBs) per water molecule and number of acceptor H bonds per OH^- in the bulk and interfacial layer of water. (e) Radial distribution function $g_{O^*C^*}(r)$ of the separation distance between C of the methyl group of hexane and O of OH^- in bulk water (seen in 0–18 ps) and in the interfacial water layer (seen in 18–36 ps).

by dynamical embedding of the tetrahedral H-bonding network, the hypercoordination in the bulk is frequently converted into a transient tetrahedral-like solvation structure (three-coordinated OH^-) that allows rapid PT and diffusion of OH^- [1] [Fig. 3(c) shows the hexane-water interfacial structure with both hypercoordinated and three-coordinated OH^-). This is the reason for the frequent PTs (spikes) between 0 and 18 ps in Fig. 3(a) and the associated high mobility of OH^-.

Our AIMD simulations showed that at ~18 ps, through one successful PT, OH^- can be brought to the hexane-water interface. Thereafter, the mobility is greatly reduced because the PT becomes rare, as seen in Fig. 3(a) for the time period from 18 to 36 ps. Specifically, the average time for a single PT event to occur is 0.87 and 5.56 ps in the bulk and at the interface, respectively. The OH^- then appears to prefer staying in the interfacial layer with no more successful PT events, as indicated by the residence probability of OH^- in the same time period of 18 to 36 ps in Fig. 3(b). The lone electron pair on OH^- is hydrophilic. Therefore, OH^- tends to accept more than three H bonds from surrounding water molecules and forms the hypercoordinated structure. However, in the condensed phase, the same water molecules are also attracted by a competing H-bonding force that is applied by the embedded liquid water structure, which largely revises the energetics of the solvation structures. Solvated in bulk water, the hydration structure is more adapted to the tetrahedral structure of water, which is active for PT. However, in the interfacial region [defined as within 5 Å from the instantaneous water surface in Fig. 3(a)], the above tetrahedral structure is largely disrupted as evidenced by the reduced average number of H bonds per water molecule from 3.80 in the bulk to 3.48 in the interface [Fig. 3(d)]. The weakened H-bonding network in the interfacial water tilts the balance of the above competition. The surrounding water molecules become more attractive to OH^- and form a hypercoordinated structure as seen by the increased average acceptor H bonds for OH^- from 3.68 in the bulk to 4.21 in the interface [Fig. 3(d)]. The largely stabilized hypercoordinated solvation structure inhabits the PT transfer for an average time of ~18 ps until it diffuses away into the bulk through a successful PT event, resulting in reduced mobility of the OH^-, which effectively traps the OH^- in the interfacial water as we observed in experiment. Moreover, the OH^- at the interfacial water is strongly correlated to hexane molecules, as evidenced by the radial distribution function $g_{O^*C^*}(r)$ of the separation distance between O^* of OH^- and C^* in the methyl group of a neighboring hexane molecule shown in Fig. 3(e) It indicates that the disrupted H-bonding network in a water-hydrophobic interface is closely associated with the presence of the hexane molecules. It is very interesting to notice that when hexane was replaced by hydrophilic molecules, such as long-chain alcohol, our experiments found no preference of OH^- appearing at the interface, in agreement with Ref. [43], because in this case the interfacial water H-bonding network remains tetrahedral-like, and the OH^- retains its high mobility with frequent PT events.

Conclusion.—In summary, we studied the propensity of OH^- at the hexane gas-water interface. Experimentally, sum-frequency vibrational spectroscopy provided clear evidence that hexane on water effectively induces the adsorption of OH^- to the interface. Hexane coverage and maximum surface density of OH^- have a one-to-one relation; roughly, a minimum of five adsorbed hexane molecules can accommodate adsorption of one OH^-. Theoretically, our AIMD simulations showed that an excess of OH^- at the interface is caused by a more stable OH^--incorporated, hypercoordinated, interfacial H-bonding network of water modified by adsorbed hexane molecules. This interfacial structure reduces the PT rate and mobility of OH^- and greatly suppresses diffusion of OH^- from the interface into the bulk. The enhanced OH^- density at the monolayer hexane-water interface suggests that hydrophobic interfaces of hydrocarbons and water are generally basic.

We especially thank Professor Yuen Ron Shen for helpful discussions and valuable comments on the manuscript. C. S. T. acknowledges support from the National Natural Science Foundation of China (Grant No. 11874123) and the National Key Research and Development Program of China (Grant No. 2016YFA0300902). X. W. is supported by the Computational Chemical Center; Chemistry in Solution and at Interfaces is funded by the Department of Energy under Award No. DE-SC0019394. This research used resources of the National Energy Research Scientific Computing Center (NERSC), a U.S. Department of Energy Office of Science User Facility operated under Contract No. DE-AC02-05CH11231.

S. Y. and M. C. contributed equally to this work.

*Corresponding author.
xifanwu@temple.edu
†Corresponding author.
cstian@fudan.edu.cn

[1] M. E. Tuckerman, A. Chandra, and D. Marx, Acc. Chem. Res. **39**, 151 (2006).
[2] C. Tanford, Science **200**, 1012 (1978).
[3] L. Escobar, M. J. Root, and R. Mackinnon, Biochemistry **32**, 6982 (1993).
[4] E. M. Knipping, M. J. Lakin, K. L. Foster, P. Jungwirth, D. J. Tobias, R. B. Gerber, D. Dabdub, and B. J. Finlayson-Pitts, Science **288**, 301 (2000).
[5] Y. Jung and R. A. Marcus, J. Am. Chem. Soc. **129**, 5492 (2007).
[6] K. G. Marinova, R. G. Alargova, N. D. Denkov, O. D. Velev, D. N. Petsev, I. B. Ivanov, and R. P. Borwankar, Langmuir **12**, 2045 (1996).

[7] J. K. Beattie and A. M. Djerdjev, Angew. Chem., Int. Ed. Engl. **43**, 3568 (2004).
[8] R. Zimmermann, N. Rein, and C. Werner, Phys. Chem. Chem. Phys. **11**, 4360 (2009).
[9] R. Zimmermann, U. Freudenberg, R. Schweiss, D. Kuettner, and C. Werner, Curr. Opin. Colloid Interface Sci. **15**, 196 (2010).
[10] C. S. Tian and Y. R. Shen, Proc. Natl. Acad. Sci. U.S.A. **106**, 15148 (2009).
[11] H. Fang, W. Wu, Y. J. Sang, S. L. Chen, X. F. Zhu, L. B. Zhang, Y. Y. Niu, and W. Gan, RSC Adv. **5**, 23578 (2015).
[12] S. Ye, S. Nihonyanagi, and K. Uosaki, Phys. Chem. Chem. Phys. **3**, 3463 (2001).
[13] A. J. Hopkins, C. L. McFearin, and G. L. Richmond, J. Phys. Chem. C **115**, 11192 (2011).
[14] K. Roger and B. Cabane, Angew. Chem., Int. Ed. Engl. **51**, 5625 (2012).
[15] E. Tyrode and J. F. D. Liljeblad, J. Phys. Chem. C **117**, 1780 (2013).
[16] R. Zangi and J. Engberts, J. Am. Chem. Soc. **127**, 2272 (2005).
[17] V. Knecht, Z. A. Levine, and P. T. Vernier, J. Colloid Interface Sci. **352**, 223 (2010).
[18] R. Vacha, S. W. Rick, P. Jungwirth, A. G. F. de Beer, H. B. de Aguiar, J. S. Samson, and S. Roke, J. Am. Chem. Soc. **133**, 10204 (2011).
[19] J. K. Beattie, Lab Chip **6**, 1409 (2006).
[20] K. Roger and B. Cabane, Angew. Chem., Int. Ed. Engl. **51**, 12943 (2012).
[21] N. Agmon, H. J. Bakker, R. K. Campen, R. H. Henchman, P. Pohl, S. Roke, M. Thamer, and A. Hassanali, Chem. Rev. **116**, 7642 (2016).
[22] Q. Du, E. Freysz, and Y. R. Shen, Science **264**, 826 (1994).
[23] L. F. Scatena, M. G. Brown, and G. L. Richmond, Science **292**, 908 (2001).
[24] M. E. Tuckerman, D. Marx, and M. Parrinello, Nature (London) **417**, 925 (2002).
[25] K. N. Kudin and R. Car, J. Am. Chem. Soc. **130**, 3915 (2008).
[26] M. Chen, L. Zheng, B. Santra, H.-Y. Ko, R. A. DiStasio, Jr., M. L. Klein, R. Car, and X. Wu, Nat. Chem. **10**, 413 (2018).
[27] X. Zhuang, P. B. Miranda, D. Kim, and Y. R. Shen, Phys. Rev. B **59**, 12632 (1999).
[28] N. Ji, V. Ostroverkhov, C. S. Tian, and Y. R. Shen, Phys. Rev. Lett. **100**, 096102 (2008).
[29] See Supplemental Material at http://link.aps.org/supplemental/10.1103/PhysRevLett.125.156803 for SFVS and AIMD simulation setup, SF spectra fitting, orientation analysis of surface species, contamination testing for hydrophobic molecule used in this work, derivation of surface charge density and OH- adsorption energy from double layer theory.
[30] C. S. Tian and Y. R. Shen, Surf. Sci. Rep. **69**, 105 (2014).
[31] Y. R. Shen, *Fundamentals of Sum-Frequency Spectroscopy* (Cambridge University Press, Cambridge, England, 2016).
[32] S. Strazdaite, J. Versluis, E. H. Backus, and H. J. Bakker, J. Chem. Phys. **140**, 054711 (2014).
[33] C. Hirose, H. Yamamoto, N. Akamatsu, and K. Domen, J. Phys. Chem. **97**, 10064 (1993).
[34] H.-F. Wang, W. Gan, R. Lu, Y. Rao, and B.-H. Wu, Int. Rev. Phys. Chem. **24**, 191 (2005).
[35] C. Hirose, N. Akamatsu, and K. Domen, J. Chem. Phys. **96**, 997 (1992).
[36] C. D. Stanners, Q. Du, R. P. Chin, P. Cremer, G. A. Somorjai, and Y. R. Shen, Chem. Phys. Lett. **232**, 407 (1995).
[37] Y. C. Wen, S. Zha, X. Liu, S. Yang, P. Guo, G. Shi, H. Fang, Y. R. Shen, and C. Tian, Phys. Rev. Lett. **116**, 016101 (2016).
[38] A. W. Adamson and A. P. Gast, *Physical Chemistry of Surfaces*, 6th ed. (John Wiley & Sons, Inc., New York, 1997).
[39] L. Zhang, C. Tian, G. A. Waychunas, and Y. R. Shen, J. Am. Chem. Soc. **130**, 7686 (2008).
[40] Y. R. Shen, Annu. Rev. Phys. Chem. **64**, 129 (2013).
[41] S. Ong, X. Zhao, and K. B. Eisenthal, Chem. Phys. Lett. **191**, 327 (1992).
[42] V. Ostroverkhov, G. A. Waychunas, and Y. R. Shen, Chem. Phys. Lett. **386**, 144 (2004).
[43] Y.-C. Wen, S. Zha, C. Tian, and Y. R. Shen, J. Phys. Chem. C **120**, 15224 (2016).
[44] M. J. Connolly, M. W. Roth, P. A. Gray, and C. Wexler, Langmuir **24**, 3228 (2008).
[45] R. Car and M. Parrinello, Phys. Rev. Lett. **55**, 2471 (1985).
[46] D. Vanderbilt, Phys. Rev. B **41**, 7892 (1990).
[47] A. D. Becke, Phys. Rev. A **38**, 3098 (1988).
[48] C. T. Lee, W. T. Yang, and R. G. Parr, Phys. Rev. B **37**, 785 (1988).
[49] D. Marx, ChemPhysChem **7**, 1848 (2006).
[50] D. Marx, A. Chandra, and M. E. Tuckerman, Chem. Rev. **110**, 2174 (2010).